International Journal of Heat and Mass Transfer 107 (2017) 450–460

Contents lists available at ScienceDirect

International Journal of Heat and Mass Transfer

journal homepage: www.elsevier.com/locate/ijhmt

Impacts of potential models on calculating the thermal conductivity of graphene using non-equilibrium molecular dynamics simulations

Chao Si [a,b], Xiao-Dong Wang [a,b,*], Zhen Fan [c], Zhi-Hai Feng [c], Bing-Yang Cao [d,*]

[a] Research Center of Engineering Thermophysics, North China Electric Power University, Beijing 102206, China
[b] School of Energy Power and Mechanical Engineering, North China Electric Power University, Beijing 102206, China
[c] Key Laboratory of Advanced Functional Composite Materials, Aerospace Research Institute of Materials and Processing Technology, Beijing 100076, China
[d] Key Laboratory for Thermal Science and Power Engineering of Ministry of Education, Department of Engineering Mechanics, Tsinghua University, Beijing 100084, China

ARTICLE INFO

Article history:
Received 17 July 2016
Accepted 16 November 2016

Keywords:
Molecular dynamics
Interatomic potential
Thermal conductivity
Graphene
Multi-layer

ABSTRACT

This work employs non-equilibrium molecular dynamics (NEMD) simulations to examine the applicability of four kinds of interatomic potential models: the Tersoff, the REBO, the opt-Tersoff and the AIREBO, which are widely used to model the thermal transport in single- and multi-layer graphene, as well as graphite crystallites. Thermal conductivities of $\sim 17 \times 5$ nm^2 and $\sim 50 \times 5$ nm^2 graphene are calculated in the temperature range of 200∼500 K with the four potentials and quantum correction is applied due to an extremely high Debye temperature of about 2100 K for graphene. The predicted thermal conductivities are compared with experimental data and phonon spectrum functions are calculated to quantify the degree of phonon scattering. The results show that two original potentials, the Tersoff and the REBO, as well as the AIREBO significantly underestimate thermal conductivities of single-layer graphene but they can qualitatively describe the trend of thermal conductivities with temperature. The opt-Tersoff is found to be the most suitable potential for modeling the thermal conductivity of both single- and multi-layer graphene because it predicts a larger frequency range and a larger frequency value for the high frequency peak, while appropriately capturing phonon scattering in thicker multi-layer graphene when Lennard-Jones term is added into the opt-Tersoff to describe interlayer atomic interactions.

1. Introduction

Carbon/carbon composites, or carbon fiber reinforced carbon composites, have been extensively utilized in aerospace and military applications [1], such as fins of ballistic missiles [2], nose cones and wing edges on aerospace vehicles [3], and rocket components [4]. The range of its civilian applications is also expanded recently, such as heat sinks, turbine rotors, and high-temperature engine [5], where the extremely high thermal conductivity, low coefficient of thermal expansion, and good mechanical strength are advantageous factors. For instance, a thermal conductivity of ~ 800 W m^{-1} K^{-1} at ~ 300 K [6] can be offered, which can also maintain the magnitude in high temperature environment (∼2000 K). The excellent thermophysical properties are highly related to microstructural features of materials, especially orientations and arrangements of graphite crystallites in carbon/carbon composites [7].

Graphite crystallites are typical nano-structures in carbon/carbon composites. As shown in Fig. 1(a), carbon layers are characterized by parallel lines and several parallel carbon layers form a graphene-like micro-crystallite (Fig. 1(b)). Every carbon layer can be regarded to be a single-layer graphene which is composed of periodical lattices of hexagonally arranged carbon atoms [1]. Yuan et al. [6] have verified that the sheet size and the number of layers significantly affect the thermal conductivities of graphite crystallites, and hence the thermal conductivity of carbon/carbon composites increases from ∼40 to ∼860 W m^{-1} K^{-1} since the average crystal coherence length L_a increases from 8 nm to 78 nm.

The measurement of thermal conductivity for the single-layer and the multi-layer graphene is very challenging due to their atom-scale thickness. Several experimental studies [8–12] have been carried out to measure the thermal conductivity of graphene, but the measured values strongly depend on sample quality, sample size, and experimental strategy. Especially, for Raman techniques, improper laser absorption rate will affect the accuracy of

* Corresponding authors at: Research Center of Engineering Thermophysics, North China Electric Power University, Beijing 102206, China (X.-D. Wang).
E-mail addresses: wangxd99@gmail.com (X.-D. Wang), caoby@tsinghua.edu.cn (B.-Y. Cao).

http://dx.doi.org/10.1016/j.ijheatmasstransfer.2016.11.065
0017-9310/

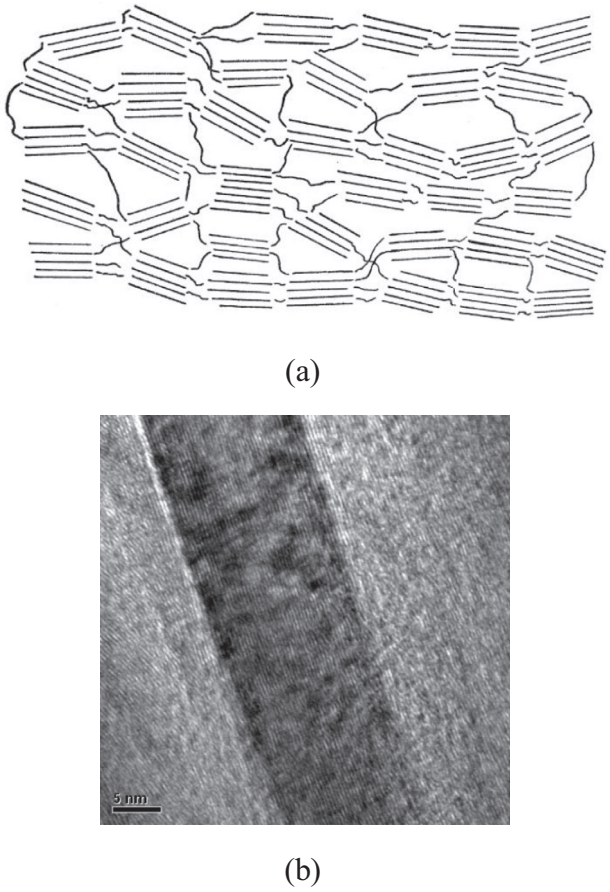

Fig. 1. (a) Schematic of graphite crystallites in C/C composites [7]; and (b) SEM image of graphite crystallite.

thermal conductivity. Consequently, modeling and simulation have been become an important tool for the understanding of their thermal properties, including Molecular dynamics (MD) simulations [13–28], non-equilibrium Green's functions (NEGF) simulations [29–32], and Boltzmann transport equation (BTE) simulations [33–36]. MD simulation is a classical technique which overestimates the specific heat below the Debye temperature (~2100 K for graphene [37]) since quantum effects are neglected in MD studies, and has some discrepancy with BTE studies in prediction of thermal conductivity [38]. BTE method has the advantage of studying large system, but the phonon-dispersion curve is needed in advance, which limits its applications. There are many situations where the phonon-dispersion curve is hardly to obtain, especially the graphene in these studies are not ideal or suspended. Moreover, the *n*-phonon process for $n>3$ has to be ignored in BTE method, which may cause system errors when predicting thermal conductivities of graphene. NEGF can be another way to study the same effects on the thermal properties. However, NEGF approach is difficult to implement when the anharmonic interactions is involved [39]. Unfortunately, the effects of anharmonic interactions are important to thermal properties of a nanomaterial. Thus, MD simulations have been extensively used to analyze the effects of atomistic changes on the thermal properties of a nanomaterial, since the *n*-phonon process and anharmonic interaction can be involved.

Technically, MD simulations employ atomic interactions as a force field and atomic motions can be followed by solving classic Newtonian equations, which have been widely used to reveal properties of molecular materials. Recently, MD simulations were used to investigate the thermal transport in graphene and graphene nano-ribbon [16–28]. As listed in Table 1, non-equilibrium molecular dynamics (NEMD) is commonly used, since the thermal conductivity of materials can be directly calculated by Fourier's law. It is worth noting that NEMD simulations have provided atomistic insights into graphene heat flow, as well as novel routes for tailoring the thermal properties of nanostructured graphene materials [38].

MD simulations require interatomic potentials that properly account for interactions between atoms. For the graphene-related materials such as multi-layer graphene and graphite crystallite, intralayer and interlayer interactions both play decisive roles in predicting their thermal conductivity. For single-layer graphene, several different potential models were employed in the previous works [16–26], as shown in Table 1. Among these models, The Tersoff [40–42] is a traditional potential developed for modeling the energetics of covalent systems with classical inter-atomic potentials. Reactive empirical bond order (REBO) potential [43] is the Tersoff type potential developed for simulating the chemical vapor deposition of diamond. The Tersoff and the REBO potentials have been used to predict the thermal conductivity of single-layer [16,23] and multi-layer [27,28] graphene materials. The two models are both empirical interatomic potentials; however, their potential parameters were not fitted from graphene-related materials. Later, an optimized model referred to as the opt-Tersoff was developed by Lindsay and Broido [44] based on the Tersoff potential, which was aimed at modeling thermal transport in graphene and carbon nano-tube. Stuart et al. [45] extended the REBO potential to the adaptive intermolecular form (AIREBO) for modeling intermolecular interactions and chemical reactions in condensed-phase hydrocarbon systems such as graphite, hydrocarbons, and polymers. It is surprising that, although the improved potentials have been developed, the two original forms are still used to model the thermal conductivity of graphene-related materials [23,27]. This indicates that the choice of potentials is somewhat arbitrary up to now; therefore, a comprehensive comparative study of the four potentials is necessary to clarify the potential applicability in prediction of thermal conductivity for the single-layer graphene.

For multi-layer graphene, the interlayer bonding force is defined by van der Waals interaction. The Tersoff, the REBO, and the opt-Tersoff potentials can only describe intralayer atomic force; thus an extra potential, often Lennard-Jones (L-J) potential, needs to be introduced to describe interlayer interactions when calculating thermal conductivity of multi-layer graphene by the three potentials. On the other hand, for the AIREBO potential, non-bonded interactions term and dihedral-angle interactions term have been added to the REBO potential. Therefore, the AIREBO potential can describe both interlayer van der Waals interaction and intralayer atomic force. A very recent experimental measurement [46] demonstrated that thermal conductivity of the multi-layer graphene shows significantly decreasing trends with an increase in the number of layers. Thus, for the calculation of thermal conductivity of multi-layer graphene, it is still needed to assess which potential can capture this observation.

In this work, the commonly used Tersoff and REBO potentials and their optimized forms (the opt-Tersoff and the AIREBO) are tested in the NEMD simulations. The predicted thermal conductivities are compared with the experimental data. The focus of this work is to provide a guideline for choosing appropriate interatomic potential when the thermal properties of single- and/or multi-layer graphene are evaluated by molecular dynamics simulations, and MD simulations is an appropriate method to study the applicabilities as the phonon scattering dominates the thermal transport of graphene and the effects of layer numbers can be effectively incorporated in MD simulations.

Table 1
Investigations of thermal transport in graphene.

Type	References and years	Thermal conductivity at 300 K ($W\,m^{-1}\,K^{-1}$)	Typical size	Potential model	Methodology
Single-layer graphene	[16] (2009)	~1300	$1.5 \times 5.7\ nm^2$	The REBO	NEMD
	[17] (2011)	~2900	$2.4 \times 2.5\ nm^2$	The optimized REBO	EMD
	[18] (2011)	77.3	$10.2 \times 10.2\ nm^2$	The AIREBO	NEMD
	[19] (2012)	53.6	$2.2 \times 10.2\ nm^2$	The AIREBO	NEMD
	[20] (2012)	400~1600	$5.2 \times (45\sim2280)\ nm^2$	The optimized Tersoff	NEMD
	[21] (2012)	78	$2.13 \times 10.5\ nm^2$	The AIREBO	NEMD
	[22] (2012)	3200~5200	$(9\sim27) \times (4\sim18)\ nm^2$	The AIREBO	EMD
	[23] (2013)	370~580	$10.4 \times (100\sim650)\ nm^2$	The Tersoff	NEMD
	[24] (2014)	400~1800	$5 \times (0.2\sim15)\ nm^2$	The optimized Tersoff	NEMD
	[25] (2015)	910~1655	$(10\sim300) \times 5.2\ nm^2$	The optimized Tersoff	NEMD
	[26] (2016)	128.4	$11.9 \times 18.2\ nm^2$	The REBO	NEMD
Multi-layer graphene	[27] (2011)	580~880	$5 \times (7.5\sim20)\ nm^2 \times (1\sim5)$ Layers	The Tersoff + LJ	NEMD
	[28] (2012)	200~1100	$(1\sim10) \times (10\sim20)\ nm^2 \times (1\sim5)$ Layers	The Tersoff + LJ	NEMD

2. Methodology

NEMD simulations are employed to study thermal transport behaviors of single- or multi-layer graphene sheets. The sheets have width of W, thickness of $H = nh$, and length of L, where n is the number of layer and h=3.4 Å is the interlayer distance of graphene. A one-dimensional heat flux is applied to the sheets along their length direction (x-direction), as shown in Fig. 2. The heat source and heat sink are located at hot side and cold side, respectively. Hence, the thermal conductivity is estimated based on Fourier's law

$$J_x = -\lambda \frac{\partial T}{\partial x} \tag{1}$$

where J_x is the heat flux, λ is the thermal conductivity, $\frac{\partial T}{\partial x}$ is the temperature gradient in the x-direction. The lattice constant and original dimensions of the graphene sheets used in this work are listed in Table 2.

In this work, the REBO, the AIREBO, the Tersoff, and the opt-Tersoff potentials are used to model the intralayer interactions. Detail formulas and parameters are presented in the APPENDIX. The used parameters for the REBO, the AIREBO, the Tersoff, and the opt-Tersoff come from Ref. [43], Ref. [45], Refs. [40–42], and Ref. [44], respectively. The thermal conductivity in armchair direction is considered. A constant heat flux is specified to the graphene along the x-direction, so that the temperature gradient can be measured after heat transfer reaches steady state. The atoms at both ends of the graphene sheet are kept fixed and the two near-end portions with the same width of δ = 10.6 Å are treated as hot and cold regions, as shown in Fig. 2. The boundary condition is non-periodic and shrink-wrapped (S boundary condition, SBC) at the width edges, while the periodic boundary condition (PBC) is specified to the length edges. LAMMPS package (http://lammps.sandia.gov/) [47] is used to perform all the MD simulations in this work. The time step is set as 1 fs. Simulations are firstly carried out in NVE ensemble for 100 ps which is long enough to reach an initial equilibrium for the system. The temperature at the equilibrium state is referred to as T_{MD}. The aggregate heat energy of 4 eV ps^{-1} is subsequently added/removed into/from the atoms in the hot/cold region. In fact, the addition/removal of energy is implemented by changing the velocities of the atoms in the hot/-cold region, that is, the velocity of atom i is modified as [20]

$$v_{i,new} = v_{i,old}\left(1 \pm \frac{\Delta Q_i}{\frac{1}{2}\sum_i m(v_{i,old}^2 - v_G^2)}\right) \tag{2}$$

where ΔQ_i is the amount of heat added/removed for atom i, v_G is the velocity of the center of mass. Our simulations show that it takes 2000 ps to reach a very good linear temperature profile in the graphene sheets simulated; thus, Fourier's law can be used to calculate thermal conductivities. The temperature profile is obtained by statistically sampling the average temperature in every 10 Å bin interval along x-direction. To eliminate the systematic error, the thermal conductivity is averaged every 100 ps from 2000 ps to 3000 ps for each case. Fig. 3 shows a typical temperature profile of a single-layer graphene sheet modeled by the AIREBO potential. The linearity is good enough for calculating the thermal conductivity.

In this work, T_{MD} ranges from 200 to 500 K. Since the temperature is much lower than the Debye temperature of graphene (2100 K) [37], quantum correction needs to be introduced to

Table 2
Lattice constant and original sizes of graphene simulated in this work.

Data source	Lattice constant (Å)	$L \times W\ (nm^2)$	$L \times W\ (nm^2)$
Experiment [53]	2.4599	16.894 × 4.795	50.682 × 4.795
The REBO [43]	2.460	16.901 × 4.797	50.703 × 4.797
The AIREBO [45]	2.460	16.901 × 4.797	50.703 × 4.797
The Tersoff [40–42]	2.530	17.374 × 4.937	52.122 × 4.937
The opt-Tersoff [44]	2.492	17.118 × 4.861	51.354 × 4.861

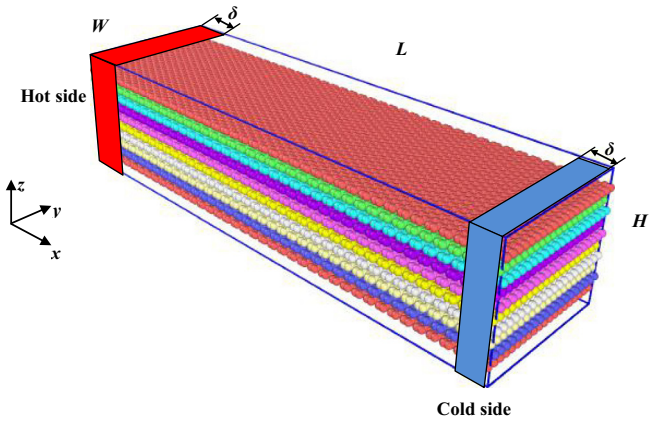

Fig. 2. Schematic of multi-layer graphene employed in this work.

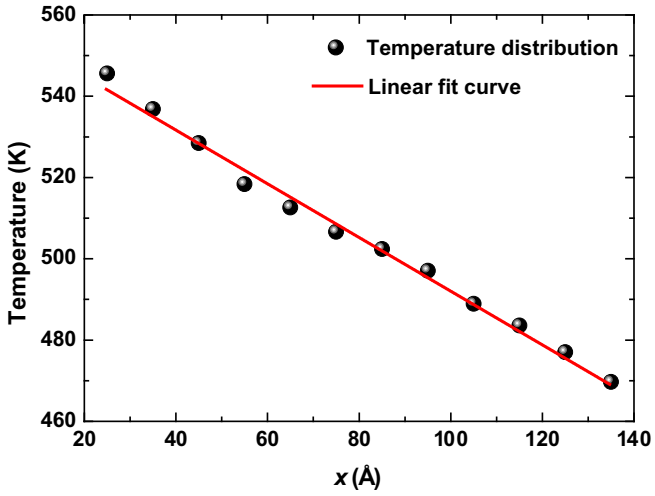

Fig. 3. A typical steady state temperature profile for a ~17 nm long graphene predicted by the AIREBO potential.

account for the quantum effect of electron. The corrected thermal conductivity λ_{cor} can be expressed as [20,48]

$$\lambda_{cor} = -\frac{J_x}{dT/dx} = -\frac{J_x}{(dT_Q/dT_{MD})(dT_{MD}/dx)} = \left(\frac{dT_{MD}}{dT_Q}\right)\lambda \tag{3}$$

where T_Q is the quantum temperature. Eq. (3) indicates that the difference between classical and quantum definitions of temperature can be considered by multiplying the thermal conductivity in Fourier's law by the factor dT_{MD}/dT_Q. The values of dT_{MD}/dT_Q can be found in Ref. [48].

To quantify the phonon spectrum in the graphene, the total phonon spectrum function $G(\omega)$ needs to be calculated based on Fourier transform of the velocity auto-correlation function (VACF) [49]

$$G(\omega) = \frac{1}{\sqrt{2\pi}} \int_0^{t_{max}} e^{i\omega t} \left\langle \sum_{j=1}^{N} v_j(t)\, v_j(0) \right\rangle dt \tag{4}$$

where $v_j(t)$ is the velocity of the jth particle at time t, ω is the vibrational wave number, and t_{max} is the sampling time of the correlation function. $G(\omega)$ indicates the amount of energy in vibrations at each frequency. Moreover, $G_z(\omega)$ is defined as the z projection of G(ω), which is the total power spectrum confined to ZA + ZO modes when the coordinate system is set as Fig. 2. Since the temperature gradient is set along x-direction for all simulated graphene, $G_z(\omega)$ can quantify most of the vibration energy transfer [49].

To reveal the phonon dispersions curves for the various potential models, the spectral energy density (SED) method developed by SED McGaughey's group [50] is utilized. The spectral energy density formula Φ can be expressed as function of the wavevector in the βth direction $\mathbf{q}_\beta$ and the frequency ω, or

$$\Phi(\mathbf{q}_\beta, \omega) = \frac{1}{4\pi\tau_0 l} \sum_{\alpha,b} m_b \left\| \int_0^{\tau_0} \sum_l \dot{u}_\alpha(l,b) \exp\left(i\mathbf{q}_\beta \cdot \mathbf{r}(l,0) - i\omega t\right) dt \right\|^2 \tag{5}$$

where m_b is the mass of atom b, l is the total number of primitive cell, τ_0 is the SED calculation time, $\dot{u}_\alpha(l,b)$ is the velocities of atom b in the α direction inside the lth cell, $\mathbf{r}(l,0)$ is the equilibrium position vector of the lth cell, i is the imaginary unit. The polarization information can be identified by dividing Φ into three directions, i.e., one out-of-plane direction and two in-plane directions.

As listed in Table 3, to validate NEMD methods used in this paper, thermal conductivity values are chosen from Refs. [19,20,23,26] as benchmarks. The REBO [26], the AIREBO [19], the opt-Tersoff [20], and the Tersoff [23] were adopted in the four references respectively. In our simulations, the sizes of the single-layer graphene and the simulation methods as well as the used potentials are set as the same as those in the respective benchmark references. The newly calculated values are compared with the literature values. Relative errors are no more than 14.0%, which is acceptable when considering the statistic fluctuation. Thus, the methods utilized in this paper are validated.

3. Results and discussion

To provide a guideline for choosing appropriate interatomic potential, thermal conductivities of single- and multi-layer graphene are predicted by the REBO, the AIREBO, the Tersoff, and the opt-Tersoff potentials and the results are compared with the experimental data. Section 3.1 examines the potential applicability for the single-layer graphene, while Section 3.2 assesses the suitable potential for the multi-layer graphene.

3.1. Single-layer graphene

Simulations are performed at 200, 250, 300, 400, and 500 K via NEMD. The sizes of the simulated single-layer graphene are ~17 × ~5 nm^2. Fig. 4 shows that thermal conductivities predicted by all the four potentials show a peak at 400 K, which can be explained by the Umklapp phonon scattering [20]. Fig. 4 also shows that thermal conductivities estimated by the opt-Tersoff potential are the highest among all the four potentials.

For single-layer graphene, the thermal conductivity is closely related to the phonon transport in the sheet. The accurate description of phonon transport is dependent on the exact modeling of the intralayer bonding force. The phonon group velocity and lifetime are two key parameters of phonon transport. In fact, when developing the opt-Tersoff potential, Lindsay and Broido [44] found that the original set of parameters for the Tersoff potential overestimates TA branch group velocities and underestimates quadratic ZA branch group velocities, so they refit the parameters based on experimental data of phonon frequencies and central Brillouin zone acoustic velocities (ZA, TA, and LA branches) of graphene. Thus, their opt-Tersoff potential describes acoustic velocities and phonon frequencies more accurately. They calculate lattice thermal conductivity of single-layer graphene by Boltzmann transport approach using the opt-Tersoff potential, and the predicted thermal conductivity shows a significant increase compared with the original Tersoff potential. Zhang et al. [17] then realized the importance of the group velocity of ZA modes phonon, which is mainly responsible for ultrahigh thermal conductivity of graphene. They demonstrated that ~43% energy of phonon heat energy is transferred via out-of-plane ZA modes at 300 K. Although ZO optical branches are overestimated in the opt-Tersoff potential, their influence on thermal conductivity can be ignored at room temperature [17].

To illustrate the different vibration status, variations of phonon spectrum for different potential models at 300 K are shown in Fig. 5. The G-band peak of the total power spectrum function $G(\omega)$ for the AIREBO, the REBO and the opt-Tersoff potentials occur at almost the same frequency, which are 4.87×10^{13}, 4.86×10^{13}, and 4.90×10^{13} Hz, respectively (Fig. 5(a)). However, for the Tersoff potential, $G(\omega)$ has no G-band peak, so the Tersoff potential cannot predict the phonon dispersion accurately. Fig. 5(b) shows the power spectrum of the ZA + ZO modes. The opt-Tersoff potential has the largest frequency range of ZA + ZO modes (0~3.94×10^{13} Hz, where the cutoff frequency is defined as a frequency at which the amplitude of ZA + ZO modes is less than

Table 3
Validation of the NEMD method for REBO, AIREBO, opt-Tersoff, and Tersoff potentials.

References	Potential models	Size and chirality of single-layer graphene	Thermal conductivity at 300 K ($W m^{-1} K^{-1}$)		
			Literature	Present	Relative error
[26]	REBO	11.9×18.2 nm^2, zigzag	128.4	134.7	4.9%
[19]	AIREBO	2.4×10.5 nm^2, armchair	53.6	46.1	14.0%
[23]	Tersoff	10.4×100 nm^2, zigzag	375.0	331.9	11.5%
[20]	Opt-Tersoff	5.2×700 nm^2, armchair	1182.0	1305.4	10.4%

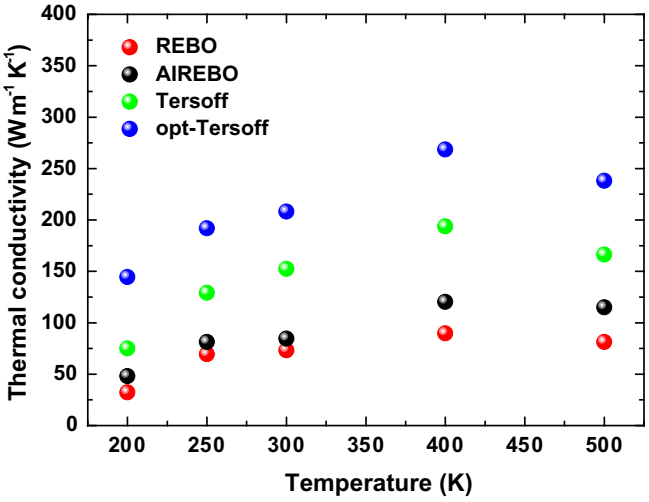

Fig. 4. Thermal conductivities predicted by REBO, AIREBO, Tersoff, and opt-Tersoff at 200, 250, 300, 400, and 500 K.

0.01). Moreover, the high frequency peak of ZA + ZO modes for the opt-Tersoff potential is located at 2.59×10^{13} Hz which is larger than that for the AIREBO potential (1.64×10^{13} Hz). However, the high frequency peak of ZA + ZO modes does not appear for the REBO potential. It can be speculated that the ZO modes disappears for the vibrations predicted by either the REBO potential or the AIREBO potential. Since most of heat energy is transferred via ZA modes, they make a remarkable contribution to the thermal conductivity of graphene [17]. As a result, the larger frequency range and the larger frequency value for the high frequency peak in the opt-Tersoff potential are two main reasons for more accurate prediction of thermal conductivity of single-layer graphene.

Fig. 6 presents the phonon dispersion curves of graphene derived from the REBO, the AIREBO, the Tersoff, and the opt-Tersoff potential models by SED method (Eq. (5)). All the adopted potential models produce a good description of certain phonon modes, where six branches can be presented. However, there exist some apparent differences from each other. The REBO and the AIREBO potentials give out similar dispersion curves except for the ZA and ZO branches. It is worth noting that the experimental frequency value of the ZO phonon at Γ point is near 2.6×10^{13} Hz. However, the value given by the REBO and the AIREBO are about 20% higher and 36% lower compared with the experimental data. Thus, in the REBO and the AIREBO potentials, the descriptions for ZO mode phonon fail. Besides, Fig. 6 gives out that the Tersoff potential fails dramatically on the in-plane optical modes, TO and LO branches. Lindsay and Broido [44] have pointed out the same result, which causes the disappearance of G-band peak in Fig. 5 (a). The opt-Tersoff gives a significant improvement of the TO and LO branches compared with the Tersoff, meanwhile keeps the ZO branch in a reasonable range. Despite an overestimation for ZO branch, the opt-Tersoff gives a good description of phonon dispersion. The physical mechanism of the differences among the phonon dispersions of the various potential models has been comprehensively discussed in the previous work of our group [51].

3.2. Multi-layer graphene

The opt-Tersoff is the most suitable potential model for NEMD to simulate the thermal transport of single-layer graphene, because it estimates the most reasonable thermal conductivity value. However, it is still unknown whether the opt-Tersoff is the best choice when simulating the thermal transport in multi-layer graphene; especially since the L-J potential is additionally coupled to it for describing the inter-layer interaction. On the other hand, although the AIREBO is proven unsuitable for modeling thermal transport in single-layer graphene, it is unclear whether its applicability will be improved for multi-layer graphene since the AIREBO inherently reflects the interlayer van der Waals interactions.

NEMD simulations are carried out to model multi-layer graphene with 1, 2, 5, 10, 20 number of layers and sheet sizes of $\sim 17 \times \sim 5$ nm^2 and $\sim 50 \times \sim 5$ nm^{2}at $T_{MD} = 500$ K. The detail sizes are shown in Table 2. It should be restated that in the REBO, the Tersoff, and the opt-Tersoff cases, L-J potential is used to describe the inter-layer interaction; while in the AIREBO case, the non-bonded interactions have already been considered so that the interlayer interaction is contained.

It is hard to directly compare the NEMD results with experimental data, because there exist magnitude difference between them due to the sizes effect of graphene sheet. Thus, the experimental observation [46] that the thermal conductivity is reduced with the number of layer is employed to examine the applicability of the four potentials. As shown in Fig. 7(a), for the two sizes of $\sim 17 \times \sim 5$ nm^2 and $\sim 50 \times \sim 5$ nm^2, the opt-Tersoff potential predicts the highest thermal conductivity. It is worth noting that only the opt-Tersoff potential can predict the reduced thermal conductivity when multi-layer graphene has larger number of layer. The inset figure in Fig. 7(a) shows that there is an apparent reduction trend with the layer number increasing from 1 to 5. The thermal conductivity of 5-layer graphene is almost the same as that of 10- and 20-layer graphene. The experimental results of Ghosh et al. [46] are shown in Fig 7(b). Ghosh et al. [46] presented that the increasing in the thickness leads to a decrease in the flux density because the number of phonon states available for three phonon modes scattering in multi-layer graphene increases as the layer number increases. Although a larger layer number provides more conduction channels in multi-layer graphene, the total phase space available for phonon scattering increases even more significantly. While in single-layer graphene there is essentially no scattering from the top and bottom surfaces, and only the edge scattering is present.

It is worth noting that Wei et al. [27], Cao et al. [28] and Lindsay et al. [52] also investigated the effects of layer number on thermal conductivity of multi-layer graphene. The works of Wei et al. [27] and Cao et al. [28] employed the Tersoff potential to model the intralayer interaction via NEMD simulations. Wei et al.'s simulations [27] showed that there is little difference in thermal conduc-

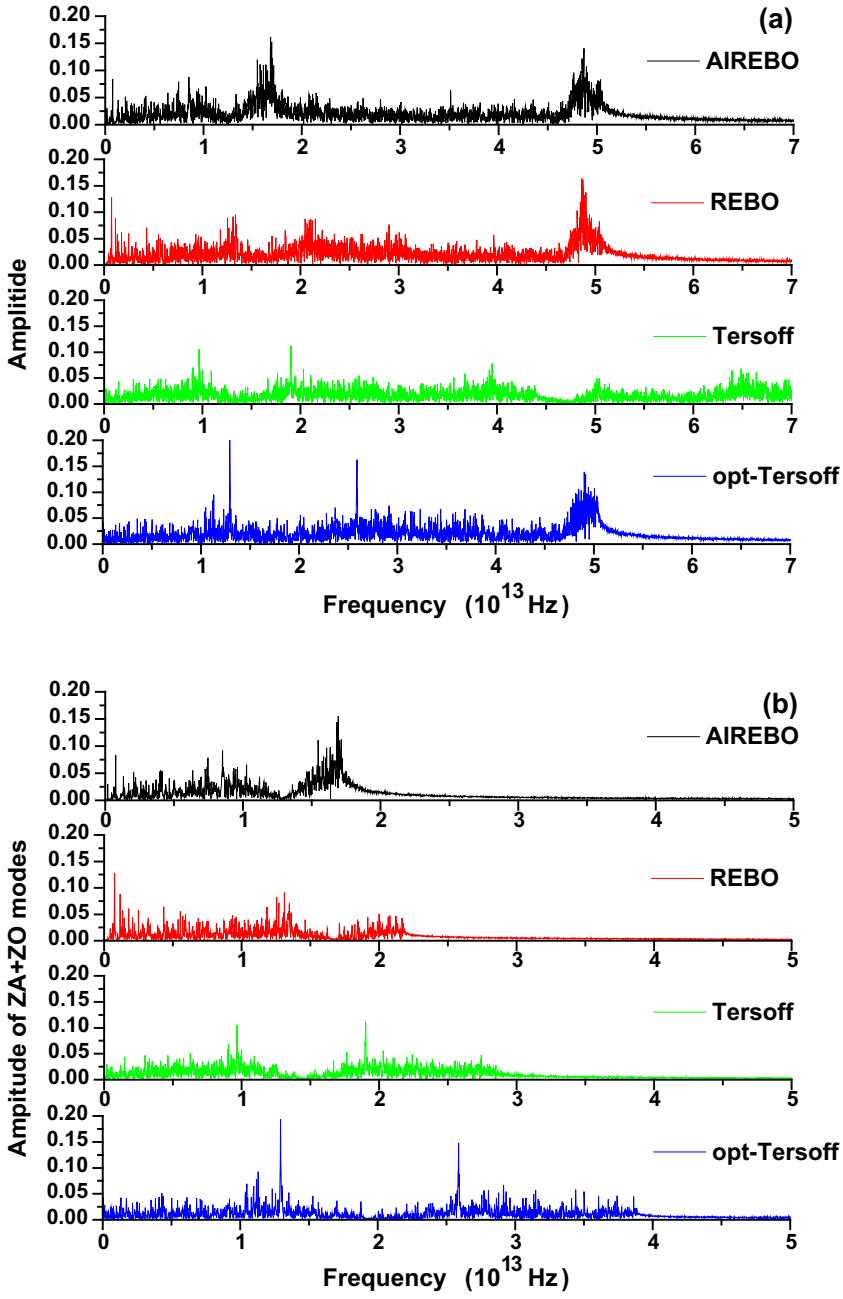

Fig. 5. Phonon spectrum functions for various potential models at 300 K: (a) total power spectrum; and (b) power spectrum of the ZA + ZO modes.

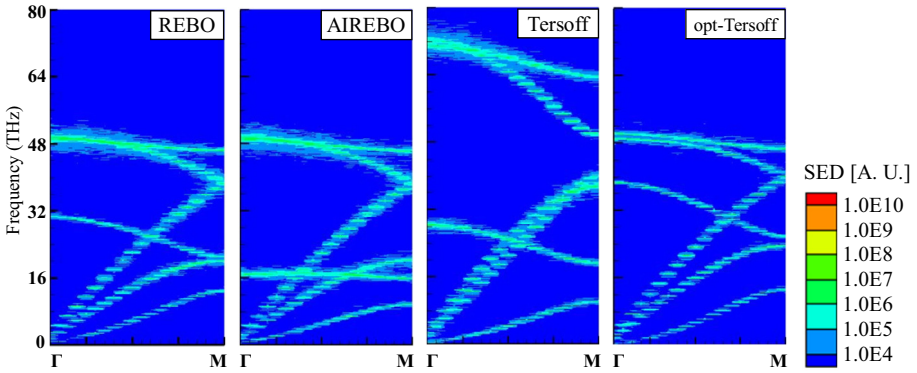

Fig. 6. Phonon dispersions of various potential models obtained by SED method.

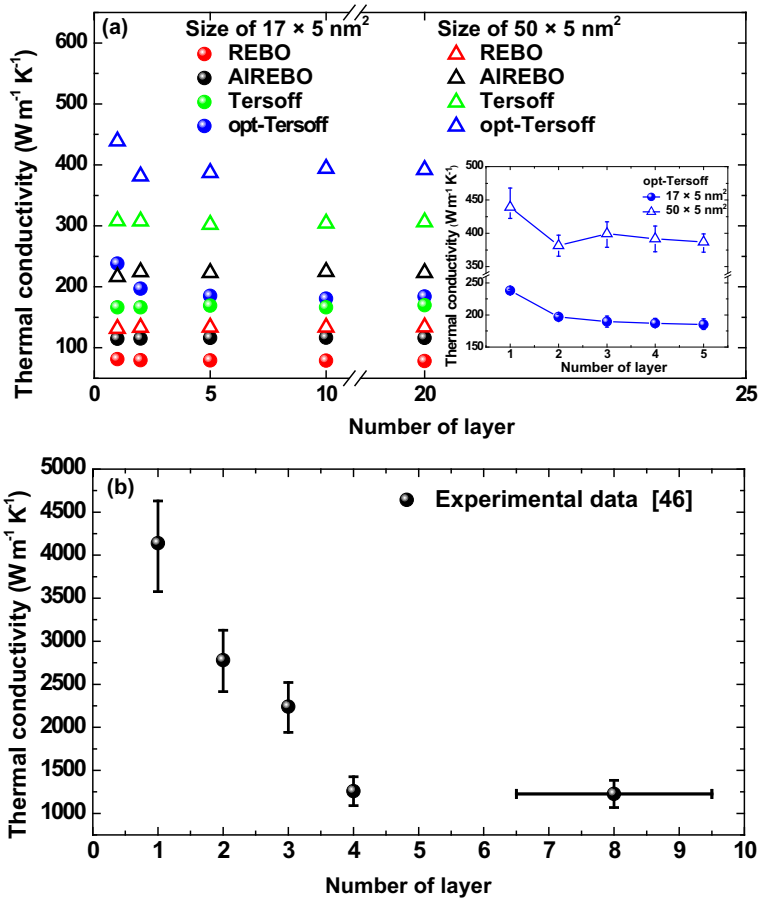

Fig. 7. Thermal conductivities of (a) multi-layer graphene with 1, 2, 5, 10, and 20 layers as well as sizes of ~17 × ~5 nm^2 and ~50 × ~5 nm^2 at T_{MD} = 500 K, and (b) multi-layer graphene with the number of layer of 1, 2, 3, 4, and 8 as well as size of ~5 × ~5 μm^2 in the experimental [46].

tivity between single-layer and five-layer graphene with the same sheet sizes of 7.5, 10, 15, and 20 × 5 nm^2, respectively. However, the thermal conductivity of 5-layer graphene is remarkably larger than that of 2-layer graphene with the sheet size of 12.5, and 25 × 5 nm^2. Temperature dependence has also been founded by Wei et al. [27], that is, the layer number has little effects on thermal conductivities at 800 K with the same sheet size, and obvious effects at 300 K. Thus, their results, which indicate the size effects and the temperature effects on the layer number dependence, may also confirm that the Tersoff potential is not appropriate for modeling the multi-layer graphene. However, Cao et al. [28] reported the decreasing trends of thermal conductivities with the increasing layer number for a 10 × 2 nm^2 multi-layer graphene. Unfortunately, the width of 2 nm in the work of Cao et al. [28] is too small, which cannot characterize the infinitely wide graphene. To verify this, we also perform additional simulations, in which multi-layer graphene with the size of ~17 × ~2 nm^2 are modeled by the Tersoff potential. The thermal conductivities also show a reduced trend with an increase in the number of layers. This result is different from that of ~17 × ~5 nm^2 counterpart. Therefore, the reduced thermal conductivity in Ref. [28] must be caused by the size effect. Lindsay et al. [52] carried out a BTE simulation to explore thermal transport for multi-layer graphene and graphite with sample length of 1~10 μm using the opt-Tersoff potential model. They also presented the result that thermal conductivity decreases monotonically with an increasing number of graphene layers until there are 5 layers. The interaction between graphene layers which breaks the graphene selection rule on phonon-phonons scattering is considered as the dominating reason for the decreasing. Lindsay et al.'s work has reasonably demonstrated the suitableness of the opt-Tersoff potential in BTE simulations when calculating the thermal conductivities of single- and/or multi-layer graphene.

To understand the scattering mechanisms in the NEMD simulations, the power spectrum function for two- and five-layer ~17 × ~5 nm^{2}graphene modeled by the opt-Tersoff potential at T_{MD} = 500 K is shown in Fig. 8. The high frequency peaks for the two-, five-layer graphene are located at almost the same frequency (4.90 × 10^{13} Hz for the two-layer graphene and 4.88 × 10^{13} Hz for the five-layer graphene). However, the amplitudes are reduced from 0.185 (two-layer graphene) to 0.168 (five-layer graphene). Similar trend is also observed for two low frequency peaks. This result verifies that there exists phonon scattering in thicker multi-layer graphene. As shown in Fig. 8(b), the interlayer atomic force also weakens frequency peaks of the ZA + ZO modes. The amplitude of high frequency peak is 0.180 for the two-layer graphene; however, it is significantly reduced to 0.096 for the five-layer graphene. The ZA + ZO modes make a remarkable contribution to the thermal conductivity of graphene; thus, the significantly reduced amplitudes of the ZA + ZO modes result in the decreased thermal conductivity when increasing the number of layer. From the side view of multi-layer graphene as shown in Fig. 8(b), an

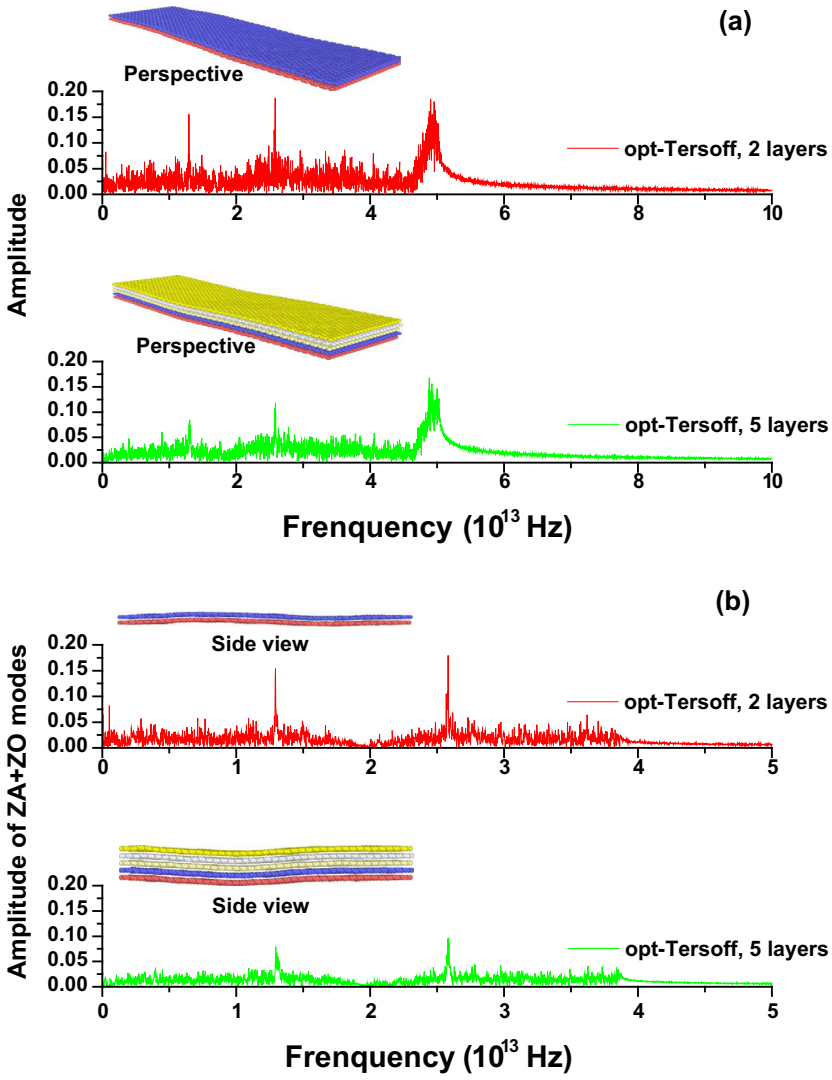

Fig. 8. Phonon spectrum function for two- and five-layer $\sim 17 \times \sim 5$ nm^2 graphene at 500 K modeled by the opt-Tersoff potentials: (a) total power spectrum; and (b) power spectrum of the ZA + ZO modes.

apparent deformation of graphene can be observed in the opt-Tersoff cases. Besides, the interlayer scattering of phonon for every layer becomes larger with the increasing layer number, which causes the decreasing thermal conductivities.

It is also found that the AIREBO potential cannot predict the phenomenon observed in Ref. [46]. As shown in Fig. 9, in the case of the AIREBO, interlayer atomic force does not exhibit significant effect on both total power spectrum energy and ZA + ZO modes power spectrum energy. In detail, for the total power spectrum, high frequency peaks for two- and five-layer graphene are located at the same frequency of 4.85×10^{13} Hz with the amplitudes of 0.177 and 0.168 (Fig. 9(a)). It is interesting that for the ZA + ZO modes power spectrum, high frequency peaks disappear for both two- and five-layer graphene. There is only a low frequency peak, which occurs at 1.79×10^{13} Hz for the two-layer graphene and at 1.76×10^{13} Hz for the five-layer graphene, the corresponding amplitudes are 0.128 and 0.116 (Fig. 9(b)). This result indicates that the AIREBO potential cannot appropriately capture interlayer phonon scattering. Thus, the AIREBO is not recommended when the thermal transport of multi-layer graphene is modeled via NEMD.

4. Conclusions

In this work, the Tersoff, the REBO, the opt-Tersoff and the AIREBO potentials are employed in NEMD simulations to model thermal transport of single- and multi-layer graphene. The predicted thermal conductivities are compared with the experimental data to search for an optimal potential. The main conclusions are as follows.

(1) For single-layer graphene, the total power spectrum function has no G-band peak when the Tersoff potential is adopted, so the Tersoff potential cannot predict the phonon dispersion accurately. Although the G-band peaks occur for the AIREBO, the REBO and the opt-Tersoff potentials, the opt-Tersoff potential predicts a larger frequency range and a larger frequency value for the high frequency peak. Moreover, the ZO modes are failure for the vibrations predicted by either the REBO potential or the AIREBO potential. Thus, thermal conductivities estimated by the opt-Tersoff potential are the highest among all the four potentials and are closer to the experimental results.

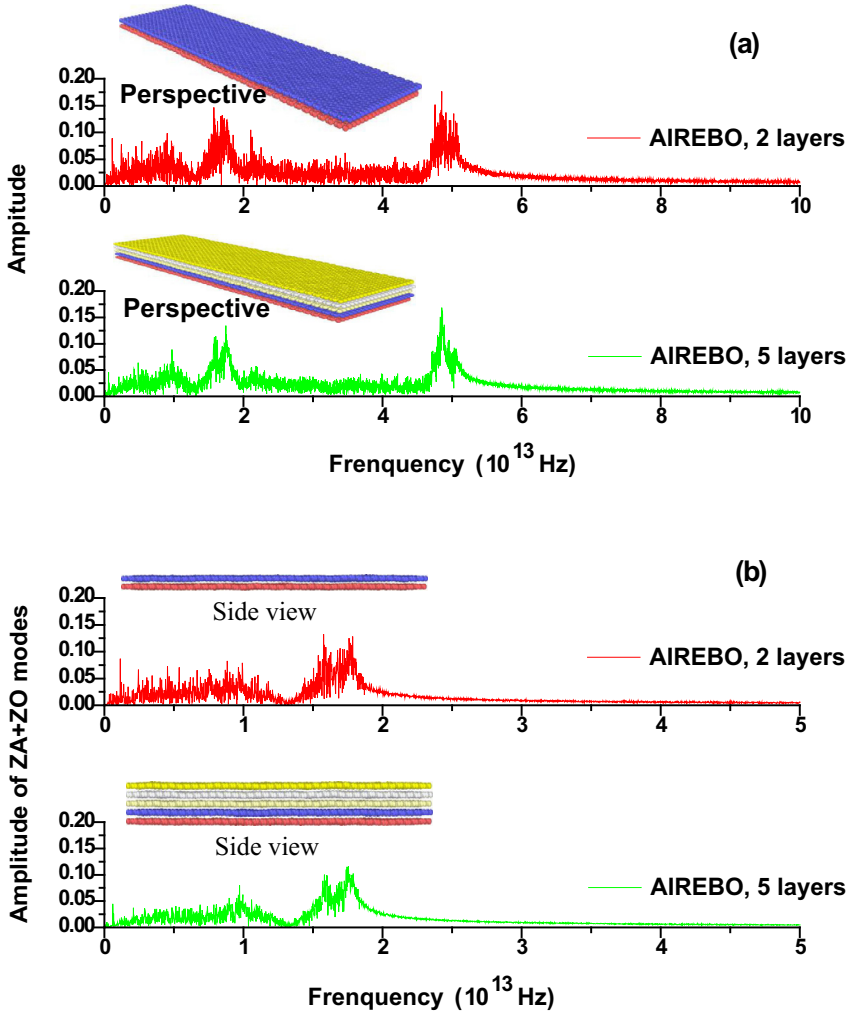

Fig. 9. Phonon spectrum function for two- and five-layer $\sim 17 \times \sim 5$ nm^2 graphene at 500 K modeled by the AIREBO potentials: (a) total power spectrum; and (b) power spectrum of the ZA + ZO modes.

(2) The experimental observation has shown that the thermal conductivity of multi-layer graphene reduces with the number of layers. Since the opt-Tersoff potential can accurately capture the significantly reduced amplitudes of the ZA + ZO modes caused by interlayer phonon scattering, it can reproduce experimental observations well. However, the AIREBO potential underestimates the interlayer phonon scattering, and hence it is not recommended when the thermal transport of multi-layer graphene is modeled via NEMD.

Acknowledgements

This study is partially supported by the National Science Fund for Distinguished Young Scholars of China (No. 51525602), and the National Science Fund of China (No. 51606064).

Appendix A

In this work, the REBO, the AIREBO, the Tersoff, and the opt-Tersoff potentials are used to model the intralayer interactions. They are described in brief as follows. The Tersoff is a 3-body potential which has been developed for modeling the energetics of covalent systems. The bond energy of atoms system modeled by the Tersoff, V_{ij}^{Tersoff}, is given by functions [40–42]

$$\begin{cases} V_{\text{ij}}^{\text{Tersoff}} = f_{ij}^{C}(f_{ij}^{R} - b_{ij}f_{ij}^{A}) \\ f_{ij}^{R} = A\mathrm{e}^{-\lambda_1 r_{ij}} \\ f_{ij}^{A} = B\mathrm{e}^{-\lambda_2 r_{ij}} \\ f_{ij}^{C} = \begin{cases} 1, & r_{ij} < R - D \\ \frac{1}{2} - \frac{1}{2}\sin\left(\frac{\pi}{2}\frac{r_{ij}-R}{D}\right), & R - D < r_{ij} < R + D \\ 0, & r_{ij} > R + D \end{cases} \\ b_{ij} = (1 + \beta^n \zeta_{ij}^n)^{-1/2n} \\ \zeta_{ij} = \sum_{k \neq i,j} f_{ik}^{C} g_{ijk} \mathrm{e}^{\lambda_3^3 (r_{ij} - r_{ik})^3} \\ g_{ijk} = 1 + \frac{c^2}{d^2} - \frac{c^2}{d^2 + (s - \cos[\theta_{ijk}])^2} \end{cases} \quad (2)$$

where r_{ij} is the length of bond between atoms i and j, f_{ij}^{A} and f_{ij}^{R} are the attractive and the repulsive pair wise terms, f_{ij}^{C} and f_{ik}^{C} is the cutoff term, R is the atomic distance at the middle of the potential well, D is the half width of the potential well, A and B are the fit parameters of energy factor, λ_1, λ_2 and λ_3 are the fit parameters of the bond length factor. The bond angle term, b_{ij}, depends on the local coordination of atoms around atom i and the angle between atoms i, j, and k. Here ζ_{ij} counts the coordination of other bonds besides the ij bond, β and n are the fit parameters of the bonds coordination. g_{ijk} is the bond bending spline function, where θ_{ijk} is the angle between atoms i, j, and k and equals 120° for graphene, c, d,

and s are the fit parameters of bond angle. The original fit parameters for the Tersoff potential are listed in Table A1.

The opt-Tersoff potential adopts the same formulas as the Tersoff potential, with two parameters being fitted to experimentally measured phonon frequencies in graphene [44]. In detail, the fitted energy factor B is optimized from 346.74 eV to 430.00 eV, and the fitted bond angle factor s is optimized from −0.57058 to −0.930, as shown in Table A2. Thus, the attractive interaction term is 1.24 times larger than that of the Tersoff, and the bond bending spline function g_{ijk} changes from 20166.89 to 741446.60, which is an increase of 36.8 times.

The REBO is a Tersoff type potential. The bond energy of atoms system modeled by the REBO, V_{ij}^{REBO}, is given by functions [43]

$$\begin{cases} V_{ij}^{\mathrm{REBO}} = f_{ij}^{C}(f_{ij}^{R} - \bar{b}_{ij} f_{ij}^{A}) \\ f_{ij}^{R} = \left(1 + \frac{Q}{r_{ij}}\right) A e^{-\alpha r_{ij}} \\ f_{ij}^{A} = \sum_{n=1}^{3} B_n e^{-\lambda_n r_{ij}} \\ f_{ij}^{C} = \begin{cases} 1, & r_{ij} < D \\ \frac{1}{2}\left(1 + \cos\frac{r_{ij}-D}{R-D}\right), & D < r_{ij} < R \\ 0, & r_{ij} > R \end{cases} \\ \bar{b}_{ij} = \frac{1}{2}(b_{ij}^{\sigma-\pi} + b_{ij}^{\pi-\sigma}) + \Pi_{ij}^{RC} + b_{ij}^{DH} \\ b_{ij}^{\sigma-\pi} = \left(1 + \sum_{k\neq i,j} f_{ik}^{C} g_{ijk}\right)^{-1/2} \\ g_{ijk} = \sum_{i=0}^{5} \beta_i \cos^i[\theta_{ijk}] \\ b_{ij}^{DH} = \frac{T_0}{2} \sum_{k,l\neq i,j} f_{ik}^{C} f_{jl}^{C} (1 - \cos^2[\Theta_{ijkl}]) \\ \cos[\Theta_{ijkl}] = \vec{\eta}_{jik} \cdot \vec{\eta}_{ijl} \\ \vec{\eta}_{jik} = \frac{\vec{r}_{ji} \times \vec{r}_{ik}}{|\vec{r}_{ji}||\vec{r}_{ik}| \sin[\theta_{ijk}]} \end{cases} \tag{3}$$

where r_{ij}, f_{ij}^{A}, f_{ij}^{R}, and f_{ij}^{C} have the same physical meanings as those in the Tersoff potential, A, B_1, B_2, and B_3 are the fit parameters of energy factor, Q, α, λ_1, λ_2 and λ_3 are the fit parameters of the bond length factor. $\bar{b}_{ij}$ is the bond angle term, $b_{ij}^{\sigma-\pi}$ is dependent on the local coordination of atoms around atom i and the bond angle θ_{ijk} between atoms i, j, and k. For graphite and graphene, $b_{ij}^{\sigma-\pi} = b_{ij}^{\pi-\sigma}$. β_i (i = 0, 1, 2, 3,4,5) in the bond bending spline function (g_{ijk})are fitted by the experimental data for graphite and diamond. Π_{ij}^{RC} is the radical energetics of vacancies, which are not considered here, i.e. $\Pi_{ij}^{RC} = 0$. b_{ij}^{DH} is a dihedral bending function and is important for describing graphene, where every third-nearest-neighbor atoms are involved in calculation. In the b_{ij}^{DH} function, $T_0$is the fit parameter, and Θ_{ijkl} is the dihedral angle of four atoms i, j,k, and l. The parameters for the REBO potential are listed in Table A3.

In the extension from REBO to AIREBO, non-bonded interactions term and dihedral-angle interactions term are added to REBO potential, that is, [45]

$$V_{kijl}^{\mathrm{AIREBO}} = \frac{1}{2}\sum_{i}\sum_{j\neq i}\left[V_{ij}^{\mathrm{REBO}} + V_{ij}^{\mathrm{LJ}} + \sum_{k\neq i,j}\sum_{l\neq i,j,k} V_{kijl}^{\mathrm{tors}}\right] \tag{4}$$

Table A1
The original fit parameters for the Tersoff potential [40–42,44].

A = 1393.6 eV	B = 346.74 eV	λ_1 = 3.4879 Å^{-1}	λ_2 = 2.2119 Å^{-1}
λ_3 = 0.0000 Å^{-1}	n = 0.72751	c = 38049.0	β = 1.5724 × 10^{-7}
d = 4.3484	s = −0.57058	R = 1.95 Å	D = 0.15 Å

Table A2
The fit parameters for the opt-Tersoff potential [44].

A = 1393.6 eV	B = 430.00 eV	λ_1 = 3.4879 Å^{-1}	λ_2 = 2.2119 Å^{-1}
λ_3 = 0.0000 Å^{-1}	n = 0.72751	c = 38049.0	β = 1.5724 × 10^{-7}
d = 4.3484	s = −0.930	R = 1.95 Å	D = 0.15 Å

Table A3
The original fit parameters for the REBO potential [43,44].

A = 10953.54 eV	B_1 = 12388.79 eV	B_2 = 17.57 eV	B_3 = 30.71 eV
α = 4.75 Å^{-1}	λ_1 = 4.72 eV	λ_2 = 1.43 eV	λ_3 = 1.38 eV
Q = 0.31346 Å	R = 2.0 Å	D = 1.7 Å	T_0 = −0.00809675
β_0 = 0.7073	β_1 = 5.6774	β_2 = 24.0970	β_3 = 57.5918
β_4 = 71.8829	β_5 = 36.2789		

where V_{ij}^{LJ} is the L-J potential term, and V_{kijl}^{tors} is the dihedral-angle term,

$$V_{ij}^{\mathrm{LJ}} = 4\varepsilon_{ij}\left[\left(\frac{\sigma_{ij}}{r_{ij}}\right)^{12} - \left(\frac{\sigma_{ij}}{r_{ij}}\right)^{6}\right] \tag{5}$$

$$V_{kijl}^{\mathrm{tors}} = \frac{1}{2}\sum_{i}\sum_{j\neq i}\sum_{k\neq i,j}\sum_{l\neq i,j,k} w_{ij}(r_{ij}) w_{jk}(r_{jk}) w_{kl}(r_{kl}) \times \varepsilon\left[\frac{256}{405}\cos^{10}\left(\frac{\Theta_{ijkl}}{2}\right) - \frac{1}{10}\right] \tag{6}$$

where σ_{ij} and ε_{ij} denote the minimum energy and the zero energy separation distance, Θ_{ijkl} is the dihedral angle, ε is the barrier height; $w_{ij}(r_{ij})$ is the bond weight, which is a number between 0 and 1, and is used as an indication of the bonding between atoms i and j.

References

[1] E. Fitzer, The future of carbon-carbon composites, Carbon 25 (2) (1987) 163–190.
[2] J.E. Sheehan, K.W. Buesking, B.J. Sullivan, Carbon-carbon composites, Annu. Rev. Mater. Res. 24 (1) (2003) 19–44.
[3] D.M. Curry, H.C. Scott, C.N. Webster, Material characteristics of space shuttle reinforced carbon-carbon, in: Proceedings of 24th National SAMPE Symposium (9th ed.), San Francisco, CA, 24(2), 1979, 1524–1539.
[4] W. Torsten, B. Gordon, Carbon-carbon: A summary of recent developments and applications, Mater. Des. 18 (1) (1997) 11–15.
[5] J. Lachaud, Y. Aspa, G.L. Vignoles, Analytical modeling of the steady state ablation of a 3D C/C composite, Int. J. Heat Mass Transfer 51 (9–10) (2008) 2614–2627.
[6] G. Yuan, X. Li, Z. Dong, X. Xiong, B. Rand, Z. Cui, Y. Cong, J. Zhang, Y. Li, Z. Zhang, J. Wang, Pitch-based ribbon-shaped carbon-fiber-reinforced one-dimensional carbon/carbon composites with ultrahigh thermal conductivity, Carbon 68 (3) (2014) 413–425.
[7] R.E. Franklin, Crystallite growth in graphitizing and non-graphitizing carbons, Proc. R. Soc. London, Ser. A 209 (1097) (1951) 196–218.
[8] A.A. Balandin, S. Ghosh, W. Bao, I. Calizo, D. Teweldebrhan, F. Miao, C.N. Lau, Superior thermal conductivity of single-layer graphene, Nano Lett. 8 (3) (2008) 902–907.
[9] W. Cai, A.L. Moore, Y. Zhu, X. Li, S. Chen, L. Shi, R.S. Ruoff, Thermal transport in suspended and supported monolayer graphene grown by chemical vapor deposition, Nano Lett. 10 (5) (2010) 1645–1651.
[10] L.A. Jauregui, Y. Yue, A.N. Sidorov, J. Hu, Q. Yu, G. Lopez, R. Jalilian, D.K. Benjamin, D.A. Delk, W. Wu, Z. Liu, X. Wang, Z. Jiang, X. Ruan, J. Bao, S.S. Pei, Y. P. Chen, Thermal transport in graphene nanostructures: Experiments and simulations, ECS Trans. 28 (5) (2010) 73–83.
[11] Y.H. Zhao, Z.K. Wu, S.H. Bai, Thermal resistance measurement of 3D graphene foam/polymer composite by laser flash analysis, Int. J. Heat Mass Transfer 101 (2016) 470–475.
[12] H.D. Wang, K. Kurata, T. Fukunaga, H. Ago, H. Takamatsu, X. Zhang, T. Ikuta, K. Takahashi, T. Nishiyama, Y. Takata, Simultaneous measurement of electrical and thermal conductivities of suspended monolayer graphene, J. Appl. Phys. 119 (24) (2016) 244306.
[13] M. Hu, D. Poulikakos, Graphene mediated thermal resistance reduction at strongly coupled interfaces, Int. J. Heat Mass Transfer 62 (4) (2013) 205–213.

[14] Y.R. Huang, P.H. Chuang, C.L. Chen, Molecular-dynamics calculation of the thermal conduction in phase change materials of graphene paraffin nanocomposites, Int. J. Heat Mass Transfer 91 (8) (2015) 45–51.
[15] A.T. Pham, M. Barisik, B.H. Kim, Interfacial thermal resistance between the graphene-coated copper and liquid water, Int. J. Heat Mass Transfer 97 (2016) 422–431.
[16] J. Hu, X. Ruan, Y.P. Chen, Thermal conductivity and thermal rectification in graphene nanoribbons: A molecular dynamics study, Nano Lett. 9 (7) (2009) 2730–2735.
[17] H. Zhang, G. Lee, K. Cho, Thermal transport in graphene and effects of vacancy defects, Phys. Rev. B 84 (11) (2011) 115460.
[18] N. Wei, L. Xu, H.Q. Wang, J.C. Zheng, Strain engineering of thermal conductivity in graphene sheets and nanoribbons: A demonstration of magic flexibility, Nanotechnology 22 (10) (2011) 105705.
[19] J.J. Yeo, Z. Liu, T.Y. Ng, Comparing the effects of dispersed Stone-Thrower-Wales defects and double vacancies on the thermal conductivity of graphene nanoribbons, Nanotechnology 23 (38) (2012) 385702.
[20] A. Cao, Molecular dynamics simulation study on heat transport in monolayer graphene sheet with various geometries, J. Appl. Phys. 111 (8) (2012) 083528.
[21] T.Y. Ng, J.J. Yeo, Z.S. Liu, A molecular dynamics study of the thermal conductivity of graphene nanoribbons containing dispersed Stone-Thrower-Wales defects, Carbon 50 (13) (2012) 4887–4893.
[22] D. Yang, F. Ma, Y. Sun, T. Hu, K. Xu, Influence of typical defects on thermal conductivity of graphene nanoribbons: An equilibrium molecular dynamics simulation, Appl. Surf. Sci. 258 (24) (2012) 9926–9931.
[23] C.X. Yu, G. Zhang, Impacts of length and geometry deformation on thermal conductivity of graphene nanoribbons, J. Appl. Phys. 113 (4) (2013) 044306.
[24] X. Xu, L.F.C. Pereira, Y. Wang, J. Wu, K. Zhang, X. Zhao, S. Bae, C.T. Bui, R. Xie, J.T. L. Thong, B.H. Hong, K.P. Loh, D. Donadio, B. Li, B. Özyilmaz, Length-dependent thermal conductivity in suspended single-layer graphene, Nat. Commun. 5 (4) (2014) 3689.
[25] L. Yang, J. Chen, N. Yang, B. Li, Significant reduction of graphene thermal conductivity by phononic crystal structure, Int. J. Heat Mass Transfer 91 (2016) 428–432.
[26] B.Y. Cao, W.J. Yao, Z.Q. Ye, Networked nanoconstrictions: An effective route to tuning the thermal transport properties of graphene, Carbon 96 (2016) 711–719.
[27] Z. Wei, Z. Ni, K. Bi, In-plane lattice thermal conductivities of multilayer graphene films, Carbon 49 (8) (2011) 2653–2658.
[28] H.Y. Cao, Z.X. Guo, H.J. Xiang, Layer and size dependence of thermal conductivity in multilayer graphene nanoribbons, Phys. Lett. A 376 (4) (2012) 525–528.
[29] Y. Xu, X.B. Chen, J.S. Wang, Thermal transport in graphene junctions and quantum dots, Phys. Rev. B 81 (19) (2010) 195425.
[30] Z. Huang, T.S. Fisher, J.Y. Murthy, Simulation of phonon transmission through graphene and graphene nanoribbons with a Green's function method, J. Appl. Phys. 108 (9) (2010) 094319.
[31] J.W. Jiang, B.S. Wang, J.S. Wang, First principle study of the thermal conductance in graphene nanoribbon with vacancy and substitutional silicon defects, Appl. Phys. Lett. 98 (11) (2011) 113114.
[32] N. Yang, X. Ni, J.W. Jiang, B. Li, How does folding modulate thermal conductivity of graphene?, Appl Phys. Lett. 100 (9) (2012) 093107.
[33] D.L. Nika, E.P. Pokatilov, A.S. Askerov, A.A. Balandin, Phonon thermal conduction in graphene: Role of Umklapp and edge roughness scattering, Phys. Rev. B 79 (15) (2009) 155413.
[34] J.H. Seol, I. Jo, A.L. Moore, A.L. Moore, L. Lindsay, Z.H. Aitken, M.T. Petters, X. Li, Z. Yao, R. Huang, D. Broido, N. Mingo, R.S. Ruoff, L. Shi, Two-dimensional phonon transport in supported graphene, Science 328 (5975) (2010) 213–216.
[35] L. Lindsay, D. Broido, N. Mingo, Flexural phonons and thermal transport in graphene, Phys. Rev. B 82 (10) (2010) 115427.
[36] Z. Aksamija, I. Knezevic, Lattice thermal conductivity of graphene nanoribbons: Anisotropy and edge roughness scattering, Appl. Phys. Lett. 98 (14) (2011) 141919.
[37] E. Pop, V. Varshney, A.K. Roy, Thermal properties of graphene: Fundamentals and applications, MRS Bull. 37 (2012) 1273–1281.
[38] L. Chen, S. Kumar, Thermal transport in graphene supported on copper, J. Appl. Phys. 112 (4) (2012) 043502.
[39] X.B. Li, K. Maute, M.L. Dunn, R.G. Yang, Strain effects on the thermal conductivity of nanostructures, Phys. Rev. B 81 (24) (2010) 245318.
[40] J. Tersoff, Modeling solid-state chemistry: Interatomic potentials for multicomponent systems, Phys. Rev. B 39 (8) (1989) 5566–5568.
[41] J. Tersoff, New empirical approach for the structure and energy of covalent systems, Phys. Rev. B 37 (12) (1988) 6991–7000.
[42] J. Tersoff, Empirical interatomic potential for carbon, with applications to amorphous carbon, Phys. Rev. Lett. 61 (25) (1988) 2879–2882.
[43] D.W. Brenner, O.A. Shenderova, J.A. Harrison, S.J. Stuart, B. Ni, S.B. Sinnott, A second-generation reactive empirical bond order (REBO) potential energy expression for hydrocarbons, J. Phys. Condens. Matter 14 (4) (2002) 783–802.
[44] L. Lindsay, D.A. Broido, Optimized Tersoff and Brenner empirical potential parameters for lattice dynamics and phonon thermal transport in carbon nanotubes and graphene, Phys. Rev. B 81 (20) (2010) 205441.
[45] S.J. Stuart, A.B. Tutein, J.A. Harrison, A reactive potential for hydrocarbons with intermolecular interactions, J. Chem. Phys. 112 (14) (2000) 6472–6486.
[46] S. Ghosh, W. Bao, D.L. Nika, S. Subrina, E.P. Pokatilov, C.N. Lau, A.A. Balandin, Dimensional crossover of thermal transport in multi-layer graphene, Nat. Mater. 9 (7) (2010) 555–558.
[47] S. Plimpton, Fast parallel algorithms for short-range molecular dynamics, J. Comput. Phys. 117 (1) (1995) 1–19.
[48] J.R. Lukes, H.L. Zhong, Thermal conductivity of individual single-wall carbon nanotubes, J. Heat Transfer 129 (6) (2007) 705–716.
[49] M. Alaghemandi, F. Leroy, F. Müller-Plathe, Thermal rectification in nanosized model systems: A molecular dynamics approach, Phys. Rev. B 81 (12) (2010) 125410.
[50] J.A. Thomas, J.E. Turney, R.M. Iutzi, C.H. Amon, A.J.H. McGaughey, Predicting phonon dispersion relations and lifetimes from spectral energy density, Phys. Rev. B 81 (8) (2010) 081411.
[51] J.H. Zou, Z.Q. Ye, B.Y. Cao, Phonon thermal properties of graphene from molecular dynamics using different potentials, J. Chem. Phys. 145 (13) (2016) 134705.
[52] L. Lindsay, D.A. Broido, N. Mingo, Flexural phonons and thermal transport in multilayer graphene and graphite, Phys. Rev. B 83 (23) (2011) 235428.
[53] Y. Baskin, L. Meyer, Lattice constants of graphite at low temperatures, Phys. Rev. 100 (2) (1955), 544–544.